

Nonlinear and Chaotic Motions for a Shock Absorbing Structure Supported by Nonlinear Springs with Hysteresis Using Fast FEA

T. Yamaguchi, Y. Kurosawa, S. Maruyama, K. Tobita, Y. Hirano, K. Yokouchi, K. Kihara, and T. Sunaga

Abstract—This paper describes dynamic analysis using proposed fast finite element method for a shock absorbing structure including a sponge. The structure is supported by nonlinear concentrated springs. The restoring force of the spring has cubic nonlinearity and linear hysteresis damping. To calculate damping properties for the structures including elastic body and porous body, displacement vectors as common unknown variable are solved under coupled condition. Under small amplitude, we apply asymptotic method to complex eigenvalue problem of this system to obtain modal parameters. And then expressions of modal loss factor are derived approximately. This approach was proposed by one of the authors previously. We call this method as Modal Strain and Kinetic Energy Method (MSKE method). Further, using the modal loss factors, the discretized equations in physical coordinate are transformed into the nonlinear ordinary coupled equations using normal coordinate corresponding to linear natural modes. This transformation yields computation efficiency. As a numerical example of a shock absorbing structures, we adopt double skins with a sponge. The double skins are supported by nonlinear concentrated springs. We clarify influences of amplitude of the input force on nonlinear and chaotic responses.

Keywords—Dynamic response, Nonlinear and chaotic motions, Finite Element analysis, Numerical analysis.

I. INTRODUCTION

TO reduce influences of external loads from precision instruments, shock absorbing structures are used. The shock absorbing structures often include springs and sponges. The springs sometimes have nonlinearity between their restoring forces and deformations under relatively large load. The sponges as air cushions are utilized to decrease impacts to human bodies. Therefore, it is of importance to clarify nonlinear dynamic motions of shock absorbing structures including elastic metal, nonlinear springs and sponges under external loads.

Dynamic responses of systems including nonlinear springs have been examined by many researchers [5], [6]. On the other hand, there are many reports [1], [2], [7]-[12] about problems having sponges using FEM or BEM. However, there exist very few studies dealing with the coupled problem between dynamic

problem of nonlinear springs with elastic structures and dynamic problems including sponges as porous materials. As an example of a shock absorbing structure, we analyze dynamic properties using finite element method for double skins with a porous material supported by nonlinear springs. The double skins are comprised of a porous material sandwiched between a rectangular thin steel panel and a thin cover plate. On the edges of the thin steel panel, we set rigid frames. The rigid frames are supported to reduce influences of external forces by nonlinear concentrated springs. The external forces are acted on a point in the steel panel. Dynamic responses at a point in the cover plate are computed.

The restoring force of the springs has cubic nonlinearity and linear hysteresis damping. Damped dynamic characteristics of air inside of the porous materials are defined by complex effective density and complex bulk modulus. Particle displacements of the internal air in the porous materials are chosen as unknowns. Displacements in the solid materials for the skins are also formulated using finite elements including complex modulus of elasticity. Thus, displacement vectors are common unknown variables for the coupled equations of motion of the shock absorbing structure. Under small amplitude, we apply asymptotic method to complex eigenvalue problem of this system to obtain modal parameters. And then expressions of modal loss factor are derived approximately. This approach was proposed by one of the authors previously. We call this method as Modal Strain and Kinetic Energy Method (MSKE method [1], [2]. Further, using the modal loss factors, the discretized equations in physical coordinate are transformed [3], [4] into the nonlinear ordinary coupled equations using normal coordinate corresponding to linear natural modes. To calculate dynamic responses, the derived equations are integrated numerically using Runge-Kutta-Gill method. This approach helps us to obtain fast computation. Influences of nonlinearity of the springs on the nonlinear and chaotic responses and the spectrums are investigated.

II. NUMERICAL MODEL

Fig. 1 shows the detail geometry of the simulation model composed of (a) double skins with a porous material, (b) rigid frames supported by nonlinear / linear concentrated springs. As shown in Fig. 1 (a), the double skins are constituted of a flat steel panel, a porous material and a steel cover plate. Thickness of the steel panel is 0.7mm. The porous material is sandwiched between the steel panel and the cover plate. Both the porous

T. Yamaguchi and S. Maruyama are with the Department of Mechanical System and Technology, Gunma University, Kiryu, Japan (e-mail: yamagme3@gunma-u.ac.jp).

Y. Kurosawa is with the Department of Mechanical and Precision Engineering, Teikyo University, Utsunomiya, Japan.

K. Tobita, Y. Hirano, K. Yokouchi, K. Kihara, and T. Sunaga are with the Graduate School of the Department of Mechanical System Engineering, Gunma University, Kiryu, Japan.

material and the cover plate are laminated on the rectangular central portion (126.0mmx112.27mm) of the steel panel. Thickness of the cover plate is 0.6mm and that of the porous material is 15mm. In the double skins, vibrations and dynamic amplitudes of the cover plate are floated due to the soft porous material. This leads to decrease impacts from the cover plate to the damped panel through the soft porous material. The length of the edges of the steel panel is 226.0mm x212.27mm. Outside of the central portion is sandwiched by the two rigid steel frames as shown in Fig. 1 (b). Thickness of the flames is 17mm. In this study, these frames can be regarded as rigid bodies because of their high stiffness. At the four corners of the bottom of the lower flame as shown in Fig. 1 (b), the flame is supported by the concentrated springs. At the corners, we set nonlinear concentrated springs in y direction (i.e. vertical direction). The concentrated nonlinear springs have cubic nonlinearity in the relation between their restoring force R_{my} and their displacement U_{my} as shown in Fig. 2. Moreover, we introduce linear hysteresis damping into the restoring force of the nonlinear springs. Namely, linear components of the spring constants have complex quantity as $\gamma_{1my} = \bar{\gamma}_{1my}(1 + j\eta_{my})$. η_{my} shows the loss factor of the springs. Further, there also exist linear concentrated springs in x and z directions (i.e. horizontal directions) at the corners.

We set the origin at the center in the xz plane on the bottom surface of the lower flame. The excitation point is $(x, y, z) = (-34.30, 17.00, 42.00)$ on the bottom surface of the steel panel. We evaluate impact responses of this simulation model. The evaluation point is $(x, y, z) = (24.95, 35.30, -35.00)$ on the cover plate.

III. NUMERICAL PROCEDURE

Next, we propose a numerical method to calculate nonlinear and chaotic responses by considering coupled damping properties for the double skins connected to the nonlinear concentrated springs as a shock absorbing structure. The double skins contain the solid materials and the porous materials. To deal with the problem having arbitrary shapes and arbitrary boundary conditions, the solid material and the porous material are modeled using finite elements. And then, they are superposed in consideration of coupled conditions. Restoring force of the nonlinear springs with linear hysteresis is formulated to connect to the double skins.

A. Discretized Equation for Nonlinear Concentrated Springs with Linear Hysteresis

First, we deal with the nonlinear concentrated springs with hysteresis. As shown in Fig. 1 (b), it is assumed that nonlinear concentrated springs with viscoelasticity have the principal elastic axes in the y direction (i.e. vertical direction). We denote the displacement as U_{my} ($m=1,2,3,\dots$) in the y direction at the nodal points α_m ($m=1,2,3,\dots$) where the nonlinear concentrated springs are connected with the frame around the double skins. Nonlinear functions using the power series are

given for the nodal forces at the points α_m . If cubic nonlinearity is considered, then the restoring forces R_{my} of the springs are expressed as

$$R_{my} = \gamma_{1my} U_{my} + \gamma_{2my} U_{my}^2 + \gamma_{3my} U_{my}^3 \quad (1)$$

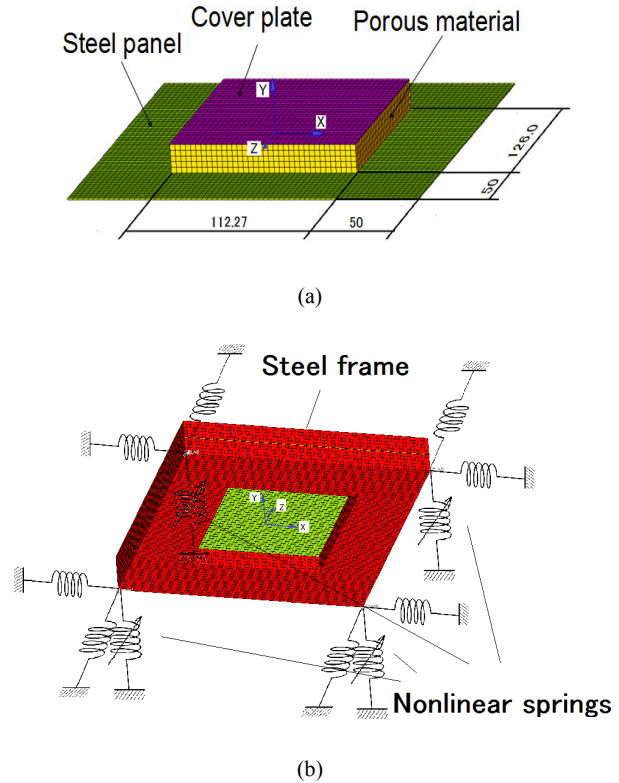


Fig. 1 Simulation model

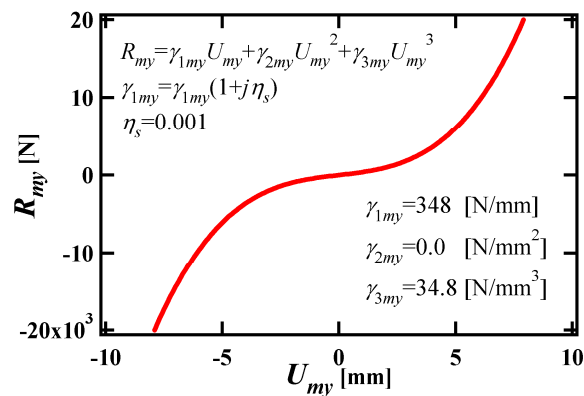


Fig. 2 Restoring force of nonlinear concentrated springs

Further, linear hysteresis damping is introduced as $\gamma_{1my} = \bar{\gamma}_{1my}(1 + j\eta_{my})$. $\bar{\gamma}_{1my}$ is the real part of γ_{1my} , and η_{1my} is the material loss factor of the concentrated spring. j is the imaginary unit. These relations can be rewritten in the matrix

form as follows [3], [4]:

$$\begin{aligned} \{R_m\} &= [\bar{\gamma}_{1m}] \{U_{sm}\} + \{\bar{d}_m\} \\ [\bar{\gamma}_{1m}] &= \begin{bmatrix} 0 & 0 & 0 \\ 0 & \gamma_{1my} & 0 \\ 0 & 0 & 0 \end{bmatrix}, \{\bar{d}_m\} = \{0, \gamma_{2my} U_{my}^2 + \gamma_{3my} U_{my}^3, 0\}^T \end{aligned} \quad (2)$$

where $\{R_m\} = \{R_{mx}, R_{my}, R_{mz}\}^T$, $R_{mx} = R_{mz} = 0$, is the nodal force vector at the node α_m . $\{U_{sm}\} = \{U_{mx}, U_{my}, U_{mz}\}^T$ is the nodal displacement vector at the node α_m . $[\bar{\gamma}_{1m}]$ is the complex stiffness matrix involving the linear term of the restoring force. $\{\bar{d}_m\}$ is the vector containing the nonlinear terms of the restoring force.

B. Discrete Equation for Double skins with Porous Material

Next, we explain modeling of the frames and the double skins with the porous material.

For the porous material in the double skins, a damped field of the internal air in the porous material is discretized using finite elements. Assuming small amplitude, equations of motion of in viscid compressive perfect fluid can be expressed as follows.

$$\text{grad } s = \rho \{ \ddot{u}_f \} \quad (4)$$

Continuity equation can be written as:

$$s = E \text{div}\{u_f\} \quad (5)$$

where particle displacement vector in the region of an element is set as $\{u_f\} = \{u_{fx}, u_{fy}, u_{fz}\}^T$. u_{fx} , u_{fy} and u_{fz} are the components of the vector in x , y and z direction, respectively. s is the force per unit area where the force s has plus quantity under expansion. Therefore, s has a relation $s = -p$ with pressure p . E and ρ are the volume elasticity and the effective density of the internal air.

Using the particle displacement vector in the region of an element $\{u_f\}$, relations between $\{u_f\}$ and particle displacement vectors $\{u_{fe}\}$ at the nodal points in the element can be approximated as follows.

$$\{u_f\} = [N_f]^T \{u_{fe}\} \quad (6)$$

where $[N_f]$ represents a matrix comprised of appropriate shape functions

We also introduce irrotational condition as $\text{rot}\{u_f\} = \{0\}$.

Next, kinetic energy, strain energy and potential energy are obtained from (4)-(6). The following expressions can be derived applying the Lagrange equation.

$$[M]_{fe} \{ \ddot{u}_{fe} \} + [K]_{fe} \{ u_{fe} \} = \{ f_{fe} \} \quad (7)$$

$$[M]_{fe} = \rho_e [\tilde{M}]_{fe} \quad (8)$$

$$[K]_{fe} = E_e [\tilde{K}]_{fe} \quad (9)$$

$\{f_{fe}\}$ is the nodal force vector. $[K]_{fe}$ is the element stiffness matrix, while $[M]_{fe}$ is the element mass matrix. ρ_e and E_e are the effective density and volume elasticity for materials in the region of the elements. $[\tilde{M}]_{fe}$ and $[\tilde{K}]_{fe}$ are the matrix consisted of the shape functions and their derivatives.

Many models for a field in porous materials have been proposed [1], [2], [7]-[12]. There exists a model using complex effective density and complex propagation speed [9]. The parameters for this model can be identified easily by improved cavity method [9] using impedance tube. In this paper, we adopt the following model using complex effective density ρ_e^* and complex volume elasticity E_e^* for the field inside the porous materials:

$$\rho_e \Rightarrow \rho_e^* = \rho_{eR} + j \rho_{eI} \quad (10)$$

$$E_e \Rightarrow E_e^* = E_{eR} + j E_{eI} \quad (11)$$

ρ_{eR} and ρ_{eI} are the real part and imaginary part of ρ_e^* , respectively. The imaginary part ρ_{eI} has a relation with flow resistance. E_{eR} and E_{eI} represent the real part and imaginary part of E_e^* , respectively. In (8), E_e^* can be easily obtained from $E_e^* = \rho_e^* (c_e^*)^2$. The authors confirmed the effectiveness of this model previously [1], [2].

By substituting (10) into (8), the element mass matrix $[M]_{fe}$ can be written as:

$$[M]_{fe} = [M_R]_{fe} (1 + j \chi_e), \chi_e = \rho_{eI} / \rho_{eR} \quad (12)$$

where $[M_R]_{fe}$ is the real part of element mass matrix $[M]_{fe}$. χ_e corresponds to the material damping due to the flow resistance. In the same manner, substitution of (11) into (9) yields the following element stiffness matrix $[K]_{fe}$.

$$[K]_{fe} = [K_R]_{fe} (1 + j \eta_e), \eta_e = E_{eI} / E_{eR} \quad (13)$$

In (13), $[K_R]_{fe}$ represents the real part of the element stiffness matrix $[K]_{fe}$. η_e shows damping effect concerning hysteresis between pressure and volume strain in the porous materials.

According to equations from (7) to (13), both the element stiffness matrix $[K]_{fe}$ and the element mass matrix $[M]_{fe}$ for internal gas in the porous materials have complex quantities

[1], [2].

Isoparametric hexahedral elements (14) are used for the porous material. The complex effective density for the porous material in this paper is set as $\rho_{eR} = 1.40 \text{ kg/m}^3$, $\chi_e = -0.500$. And the complex volume elasticity is $E_{eR} = 1.19 \times 10^5 \text{ N/m}^2$, $\eta_e = 0.100$.

For vibration of the steel panel, the cover plate and the frames, we used discretized equations written in the following equations from (14) to (18). They correspond to conventional linear finite element model in consideration of hysteresis damping. Stress-strain relation and strain-displacement relation are expressed as:

$$\{\sigma\} = [D]\{\varepsilon\} \quad (14)$$

$$\{\varepsilon\} = [A]\{u_s\} \quad (15)$$

$\{\sigma\}$ stands for the stress vector. $\{u_s\}$ is the displacement vector for the solid bodies and $\{\varepsilon\}$ is the strain vector. $[A]$ is the matrix comprised of differential operators, while $[D]$ is the matrix including modulus of elasticity and Poisson's ratio.

Using the matrix $[N_s]$ containing shape functions, relations between displacement $\{u_s\}$ in an element and displacements $\{u_{se}\}$ at nodal points are approximated as:

$$\{u_s\} = [N_s]^t \{u_{se}\} \quad (16)$$

Kinetic energy, strain energy and potential energy are calculated using (14)-(16). The following expressions can be obtained by applying the Lagrange equation.

$$[M]_{se} \{\ddot{u}_{se}\} + [K]_{se} \{u_{se}\} = \{f_{se}\} \quad (17)$$

$$[K]_{se} = [K_R]_{se} (1 + j \eta_e) \quad (18)$$

$\{f_{se}\}$ is the nodal force vector in an element e for the solid bodies, and $[K]_{se}$ and $[M]_{se}$ are the element stiffness matrix and element mass matrix, respectively.

By replacing complex modulus of elasticity with real modulus of elasticity in the matrix $[D]$ in (14), the solid bodies with damping can be modeled using finite elements. Consequently, the element stiffness matrix $[K]_{se}$ in (17) becomes to have complex quantities in (18). η_e is the material loss factor corresponding to each element e . $[K_R]_{se}$ is the real part of element stiffness matrix for the solid bodies.

For the elastic materials, isoparametric hexahedral elements with the non-conforming modes [15], [16] are selected.

C. Discrete Equation for System between the Double Skins and the Frames

All elements for the porous materials and the solid bodies in

the double skins having the frame are superposed appropriately using equations from (4) to (18). At boundaries between the solid bodies and the porous materials, normal components of the displacements to the boundaries are continuous. Tangential components of the displacements along the boundaries are independent mutually. With taking these conditions into account, the following equation can be obtained.

$$[M_a] \{\ddot{u}_a\} + [K_a] \{u_a\} = \{f_a\} \quad (19)$$

where $\{f_a\}$ is the nodal force vector and $\{u_a\}$ is the nodal displacement vector. $\{u_a\}$ is consisted of $\{u_{fe}\}$ and $\{u_{se}\}$. In the same way, $[K_a]$ includes $[K]_{fe}$ and $[K]_{se}$, while $[M_a]$ involves $[M]_{fe}$ and $[M]_{se}$.

D. Discrete Equations for the Global System between the Double Skins and the Nonlinear Springs

The restoring force $\{R_m\}$ in (2) is added to the nodal force at the attached nodes α_m between the nonlinear concentrated springs and the frame. Moreover, the linear springs are also connected. Subsequently, the following expression can be obtained for the global system:

$$[M] \{\ddot{u}\} + [K] \{u\} + \{\hat{d}\} = \{f\}, \quad \{\hat{d}\} = \sum_{m=1} \{\hat{d}_m\} \quad (20)$$

where $\{u\}$, $[M]$, $[K]$, and $\{f\}$ are the displacement vector, complex mass matrix, complex stiffness matrix, and external force vector in the global system, respectively. $\{\hat{d}_m\}$ is modified from $\{\bar{d}_m\}$ to have a vector size identical to d of the global system.

E. An Expression for Modal Damping

We propose a calculation method [1], [2] to obtain modal damping for the concentrated springs and the double walls containing the solid bodies and the porous materials in the global system. Under small deformation, we neglect the nonlinear term and the external force in (20). Further, we assume that $\{u\}$ can be written as $\{u\} = \{\phi\} e^{j\omega t}$. t and ω denote the time and the angular frequency, respectively. Consequently, we obtain homogeneous equation of (20). This corresponds to complex eigenvalue problem as:

$$\sum_{e=1}^{e_{\max}} ([K_R]_e (1 + j\eta_e) - (\omega^{(i)})^2 (1 + j\eta_{tot}^{(i)}) [M_R]_e (1 + j\chi_e)) \{\phi^{(i)}\} = \{0\} \quad (21)$$

In this equation, superscript (i) stands for the i -th eigenmode. $(\omega^{(i)})^2$ is the real part of complex eigenvalue. $\{\phi^{(i)}\}$ is the complex eigenvector and $\eta_{tot}^{(i)}$ is the modal loss factor. Next, we introduce the following β_{se} and β_{ke} using the maximum value η_{\max} among the elements' material loss factors

η_e and $\chi_e, (e=1,2,3,\dots, e_{\max})$

$$\beta_{se} = \eta_e / \eta_{\max}, |\beta_{se}| \leq 1, \beta_{ke} = \chi_e / \eta_{\max}, |\beta_{ke}| \leq 1 \quad (22)$$

On assumption of $|\eta_{\max}| \ll 1$, solutions of (21) are expanded [14], [1], [2] using a small parameter $\mu = j\eta_{\max}$:

$$\{\phi^{(i)}\} = \{\phi^{(i)}\}_0 + \mu\{\phi^{(i)}\}_1 + \mu^2\{\phi^{(i)}\}_2 + \dots \quad (23)$$

$$(\omega^{(i)})^2 = (\omega_0^{(i)})^2 + \mu^2(\omega_2^{(i)})^2 + \mu^4(\omega_4^{(i)})^2 + \dots \quad (24)$$

$$j\eta_{tot}^{(i)} = \mu\eta_1^{(i)} + \mu^3\eta_3^{(i)} + \mu^5\eta_5^{(i)} + \mu^7\eta_7^{(i)} + \dots \quad (25)$$

In these equations, under conditions of $|\beta_{se}| \leq 1, |\beta_{ke}| \leq 1$ and $|\eta_{\max}| \ll 1$, we can obtain $|\eta_{\max}\beta_{se}| \ll 1$ and $|\eta_{\max}\beta_{ke}| \ll 1$. Thus, both $\mu\beta_{se}$ and $\mu\beta_{ke}$ are regarded as small parameters like μ . In the equations, $\{\phi^{(i)}\}_0, \{\phi^{(i)}\}_1, \{\phi^{(i)}\}_2, \dots$ and $(\omega_0^{(i)})^2, (\omega_2^{(i)})^2, (\omega_4^{(i)})^2, \dots$ and $\eta_1^{(i)}, \eta_3^{(i)}, \eta_5^{(i)}, \dots$ have real quantities. Substituting equations from (23) to (25) into (21) yields approximate equations using μ^0 and μ^1 orders. The following equation can be derived by arranging the approximate equations:

$$\eta_{tot}^{(i)} = \eta_{se}^{(i)} - \eta_{ke}^{(i)} \quad \eta_{se}^{(i)} = \sum_{e=1}^{e_{\max}} (\eta_e S_{se}^{(i)}), \quad \eta_{ke}^{(i)} = \sum_{e=1}^{e_{\max}} (\chi_e S_{ke}^{(i)}) \quad (26)$$

According to these expressions, modal loss factor $\eta_{tot}^{(i)}$ can be calculated using material loss factors η_e of each element e , share $S_{se}^{(i)}$ of strain energy of each element to total strain energy, material loss factors χ_e of each element e and share $S_{ke}^{(i)}$ of kinetic energy of each element to total kinetic energy. We call this method as Modal Strain and Kinetic Energy Method, MSKE Method [1], [2], [13]. This method helps us to diminish computational time for large scaled finite element models for the shock absorbing structure.

F. Conversion from the Discretized Equation in Physical Coordinate to the Nonlinear Equation in Normal Coordinate

Considerable computational time is required to directly calculate (20) in physical coordinates. In this section, a numerical method is proposed to decrease the degree of freedom for the discretized equations of motion [3], [4].

First, we assume that the linear eigenmodes $\{\phi^{(i)}\}$ can be approximated to $\{\phi^{(i)}\}_0$. Next, by introducing normal coordinates \tilde{b}_i corresponding to the linear eigenmodes $\{\phi^{(i)}\}_0$, the nodal displacement vector can be expressed as follows:

$$\{u\} = \sum_{i=1} \tilde{b}_i \{\tilde{\phi}^{(i)}\}_0 / n_i \quad (27)$$

where $\{\phi^{(i)}\}_0 = \sqrt{m_i} \{\tilde{\phi}^{(i)}\}_0 = \{\tilde{\phi}^{(i)}\}_0 / n_i, n_i = 1/\sqrt{m_i}$,

$$m_i = \{\phi^{(i)}\}_0^T [M_R] \{\phi^{(i)}\}_0, \{\tilde{\phi}^{(i)}\}_0^T [M_R] \{\tilde{\phi}^{(i)}\}_0 = 1$$

By substitution of (27) into (20), the following nonlinear ordinary simultaneous equations with regard to normal coordinates \tilde{b}_i can be obtained.

$$\begin{aligned} \ddot{\tilde{b}}_i + \eta_{tot}^{(i)} \omega^{(i)} \dot{\tilde{b}}_i + (\omega^{(i)})^2 \tilde{b}_i + \sum_j \sum_k \tilde{D}_{ijk} \tilde{b}_j \tilde{b}_k \\ + \sum_j \sum_k \sum_l \tilde{E}_{ijkl} \tilde{b}_j \tilde{b}_k \tilde{b}_l = \tilde{P}_i \end{aligned} \quad (28)$$

$$\{\tilde{\phi}^{(i)}\}_0 = \{\tilde{\phi}_{i1x}, \tilde{\phi}_{i1y}, \tilde{\phi}_{i1z}, \tilde{\phi}_{i2x}, \tilde{\phi}_{i2y}, \tilde{\phi}_{i2z}, \tilde{\phi}_{i3x}, \dots\}^T,$$

$$\tilde{P}_i = n_i \{\tilde{\phi}^{(i)}\}_0^T \{F\}, \quad \tilde{D}_{ijk} = \sum_{m=1}^4 \tilde{\gamma}_{2my} (n_i / (n_j n_k)) \tilde{\phi}_{imy} \tilde{\phi}_{jmy} \tilde{\phi}_{kmy}$$

$$\tilde{E}_{ijkl} = \sum_{m=1}^4 \tilde{\gamma}_{3my} (n_i / (n_j n_k n_l)) \tilde{\phi}_{imy} \tilde{\phi}_{jmy} \tilde{\phi}_{kmy} \tilde{\phi}_{lmy}$$

Because (28) has a much smaller degree of freedom than (20), we can save considerable computational time. $\tilde{\phi}_{imy}$ is the y -component of the eigenmode $\{\tilde{\phi}^{(i)}\}_0$ at the m -th connected node α_m between the frame and the nonlinear concentrated springs. Note that the damping term in (28) can be derived in an identical form to (26) through this numerical manipulation.

G. Impact Response

Nonlinear responses are calculated by applying Runge-Kutta-Gill method to (28), when an external force having a cosine wave in y direction is given for the component of the force vector $\{F\}$ as $\tilde{P}_i = |F_{\max}| \cos(2\pi f_{ex} t)$ in (28) at the node β , which is excitation point as we specified in Fig. 1. f_{ex} is the frequency of the periodic force. We compute nonlinear time histories by varying the maximum amplitude $|F_{\max}|$ of the cosine external force.

IV. NUMERICAL RESULTS AND DISCUSSION

A. Eigenmodes, Resonant Frequencies and Modal Loss Factors

Figs. 3 and 4 represent resonant frequencies $\omega_0^{(i)} / (2\pi)$, modal loss factors $\eta_{tot}^{(i)}$ and eigenmodes $\{\tilde{\phi}^{(i)}\}_0$. To visualize the deformations of each layer in the double skins easily, the frames are removed from the display of the specified eigenmodes (i.e. modes 7 to 25) in Figs. 3 and 4. For the

eigenmodes in Fig. 3 from mode 1 to mode 3, deformation in the cover plate is dominant. On the other hand, deformations in the concentrated springs are large for the eigenmodes from mode 4 to mode 9. In these modes, we can regard as rigid for both the double skins and the frames. For the eigenmodes from mode 10 to mode 12, deformation of the porous material is large. In these modes, the air spring in the porous material magnifies the vibration amplitude of the cover plate. As shown in Fig. 4, the first, the second and the third flexural modes of the steel panel (i.e. lower skin) correspond to mode 18, mode 23 and mode 25, respectively. Note that the deformation of the only steel panel (i.e. lower skin) is displayed for the mode 18, mode 23 and mode 25. For the other eigenmodes in Figs. 3 and 4, we can find that the deformations of the layers are coupled complicatedly in the doubles skins.

B. Dynamic Responses under Periodic External Force

We compute dynamic responses of the shock absorbing structure when the cosine periodic force in y direction is applied upon the excitation point, which is on the bottom of the steel panel (i.e. lower skin). And the displacements w in y direction at the evaluation point on the cover plate (i.e. upper skin) are evaluated. Especially, we focus on investigations of the nonlinear motions under the 1:3 internal resonance condition between the mode 6 (i.e. the bouncing mode having dominant deformation in the nonlinear concentrated spring in y direction) and the mode 10 (i.e. the mode with the rigid motion of the cover plate in y direction having large deformations of the pneumatic spring in the porous material). These modes are expected to have nonlinear coupling motions mutually under the excitation in y direction. We fix the excitation frequency f_{ex} as 64.95 [Hz] in the vicinity of the eigen frequency of mode 6. We investigate responses of the shock absorbing structure due to nonlinear springs by varying the maximum amplitude $|F_{max}|$ of the input force. Fig. 5 (a) shows the calculated time history under small force amplitude $|F_{max}| = 0.01$ [N]. Fig. 5 (b) represents the Fourier spectrum of the time history in Fig. 5 (a). As for (m,n) in Fourier spectrum, m denotes the m -th eigenmode, while n denotes types of the spectrum. For example, $n=1/2$ shows sub-harmonic component of the $1/2$ order, and $n=3$ corresponds to super-harmonic component of the third order.

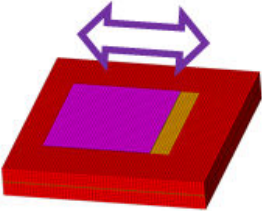
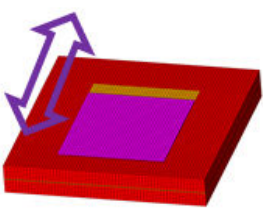
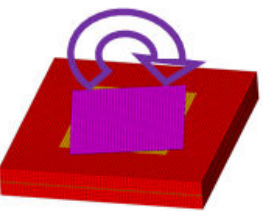
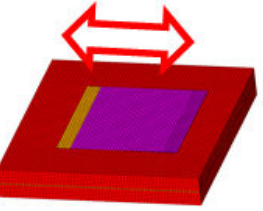
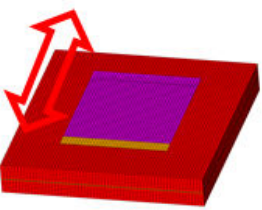
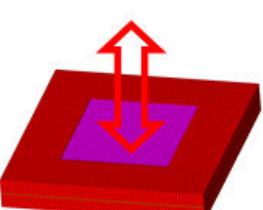
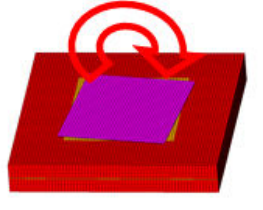

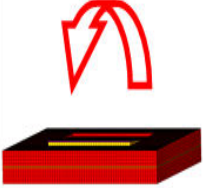
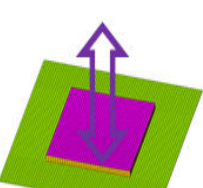
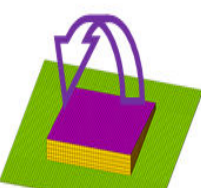

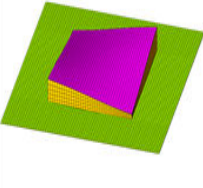
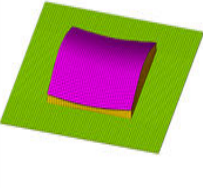
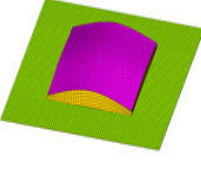
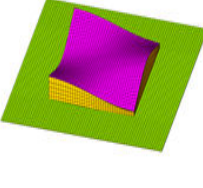
Mode 1	Mode 2	Mode 3	Mode 4
			
$f^{(1)} = 3.20\text{Hz}, \eta_{\text{tot}}^{(1)} = 0.0010$	$f^{(2)} = 3.20\text{Hz}, \eta_{\text{tot}}^{(2)} = 0.0010$	$f^{(3)} = 3.28\text{Hz}, \eta_{\text{tot}}^{(3)} = 0.0010$	$f^{(4)} = 64.2\text{Hz}, \eta_{\text{tot}}^{(4)} = 0.0010$
Mode 5	Mode 6	Mode 7	Mode 8
			
$f^{(5)} = 64.3\text{Hz}, \eta_{\text{tot}}^{(5)} = 0.0010$	$f^{(6)} = 64.9\text{Hz}, \eta_{\text{tot}}^{(6)} = 0.0011$	$f^{(7)} = 99.8\text{Hz}, \eta_{\text{tot}}^{(7)} = 0.0011$	$f^{(8)} = 100.4\text{Hz}, \eta_{\text{tot}}^{(8)} = 0.0012$
Mode 9	Mode 10	Mode 11	Mode 12
			
$f^{(9)} = 100.8\text{Hz}, \eta_{\text{tot}}^{(9)} = 0.0012$	$f^{(10)} = 195.2\text{Hz}, \eta_{\text{tot}}^{(10)} = 0.0902$	$f^{(11)} = 207.3\text{Hz}, \eta_{\text{tot}}^{(11)} = 0.0989$	$f^{(12)} = 209.2\text{Hz}, \eta_{\text{tot}}^{(12)} = 0.0993$
Mode 13	Mode 14	Mode 15	Mode 16
			
$f^{(13)} = 256.0\text{Hz}, \eta_{\text{tot}}^{(12)} = 0.0704$	$f^{(14)} = 296.6\text{Hz}, \eta_{\text{tot}}^{(14)} = 0.0568$	$f^{(15)} = 347.1\text{Hz}, \eta_{\text{tot}}^{(15)} = 0.0397$	$f^{(16)} = 418.5\text{Hz}, \eta_{\text{tot}}^{(16)} = 0.0310$

Fig. 3 Eigenmodes of shock absorbing structure (from mode 1 to mode 16)

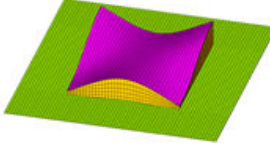
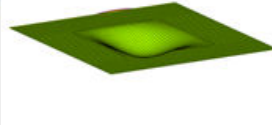
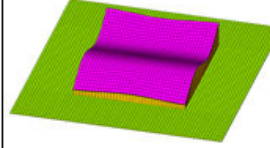
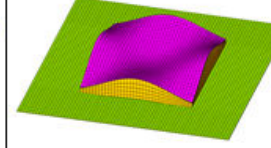
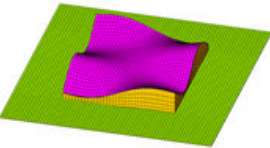
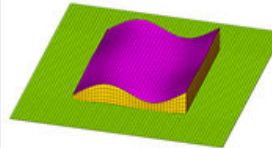
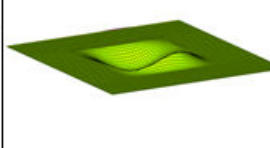
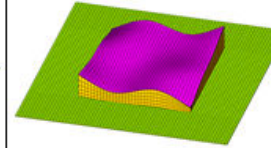
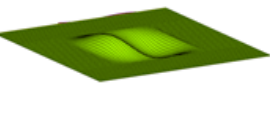
Mode 17	Mode 18	Mode 19	Mode 20
	 Lower side		
$f^{(17)} = 446.7\text{Hz}, \eta_{\text{tot}}^{(17)} = 0.0283$	$f^{(18)} = 495.3\text{Hz}, \eta_{\text{tot}}^{(18)} = 0.0235$	$f^{(19)} = 622.7\text{Hz}, \eta_{\text{tot}}^{(19)} = 0.0164$	$f^{(20)} = 715.2\text{Hz}, \eta_{\text{tot}}^{(20)} = 0.0132$
Mode 21	Mode 22	Mode 23	Mode 24
		 Lower side	
$f^{(21)} = 745.0\text{Hz}, \eta_{\text{tot}}^{(21)} = 0.0128$	$f^{(22)} = 762.5\text{Hz}, \eta_{\text{tot}}^{(22)} = 0.0123$	$f^{(23)} = 871.2\text{Hz}, \eta_{\text{tot}}^{(23)} = 0.0080$	$f^{(24)} = 887.0\text{Hz}, \eta_{\text{tot}}^{(24)} = 0.0098$
Mode 25			
 Lower side			
$f^{(25)} = 994.1\text{Hz}, \eta_{\text{tot}}^{(25)} = 0.0065$			

Fig. 4 Eigenmodes of shock absorbing structure (from mode 17 to mode 25)

From Fig. 5 (a), we can find a periodic wave having the excitation frequency $f_{\text{ex}} = 64.95\text{Hz}$ in the calculated time history. As we described previously, this frequency f_{ex} is also almost same with the eigen frequency of mode 6. The only one peak appears corresponding to f_{ex} in the Fourier spectrum. Thus, there is a rigid motion of the whole shock absorbing structure in y direction. The deformations of the nonlinear concentrated springs are dominant in this peak. This response can be regarded as a typical linear response under small input force.

Fig. 6 shows the calculated results under middle force

amplitude $|F_{\text{max}}| = 490 \text{ [N]}$. The periodic wave in Fig. 6 (a) is distorted due to the nonlinear effects of the concentrated springs. This leads to the three peaks in the Fourier spectrum in Fig. 6 (b). In the spectrum, there are super harmonic components of the third and fifth orders (i.e. (6, 3) and (6,5)) related to the eigenfrequency of mode 6. The frequencies of these peaks are also corresponding to the super harmonic components of the excitation frequency f_{ex} . Especially, the peak (6,3) also corresponds to the eigen frequency (i.e. (10,1)) of mode 10. This means that the 1:3 internal resonance is generated as we expected previously due to the nonlinearity of the concentrated springs in y direction.

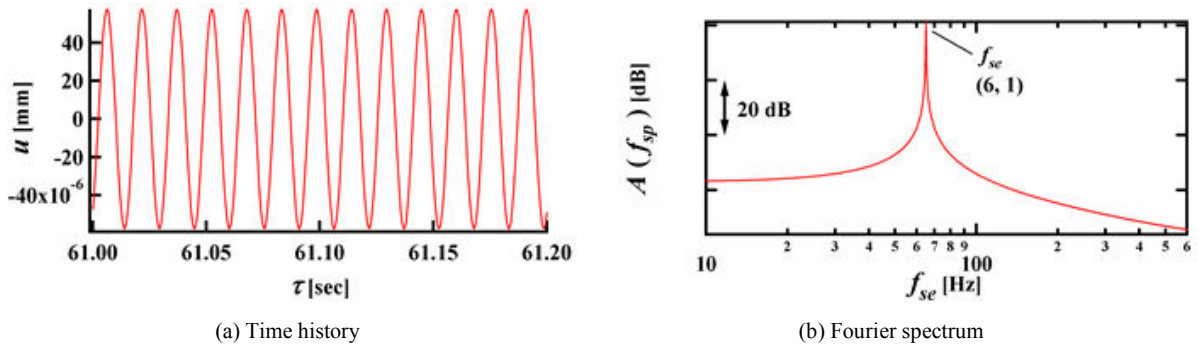


Fig. 5 Dynamic response of shock absorbing structure under small force amplitude ($f_{ex}=64.95\text{Hz}$, $|F_{\max}|=0.01\text{N}$)

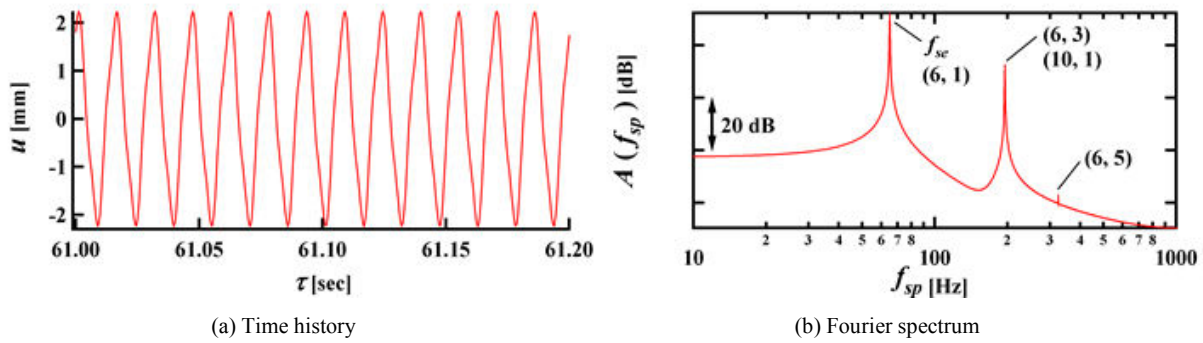


Fig. 6 Dynamic response of shock absorbing structure under middle force amplitude ($f_{ex}=64.95\text{Hz}$, $|F_{\max}|=490\text{N}$)

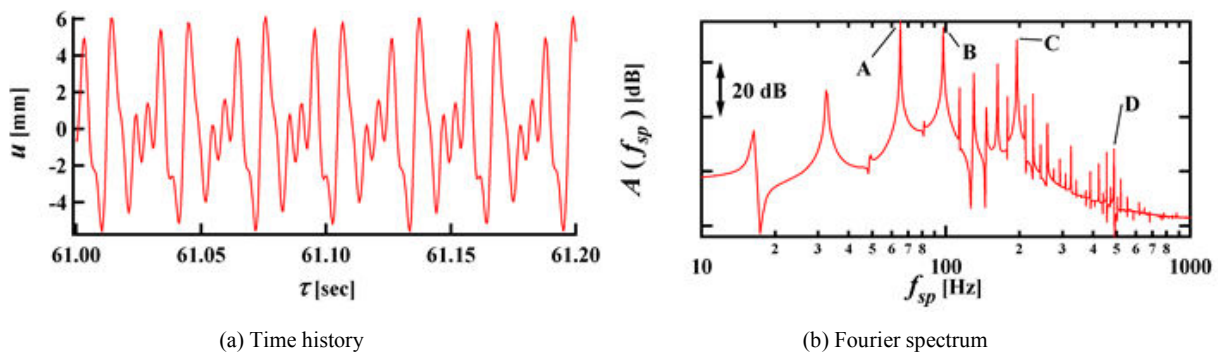


Fig. 7 Dynamic response of shock absorbing structure under large force amplitude ($f_{ex}=64.95\text{Hz}$, $|F_{\max}|=4899\text{N}$)

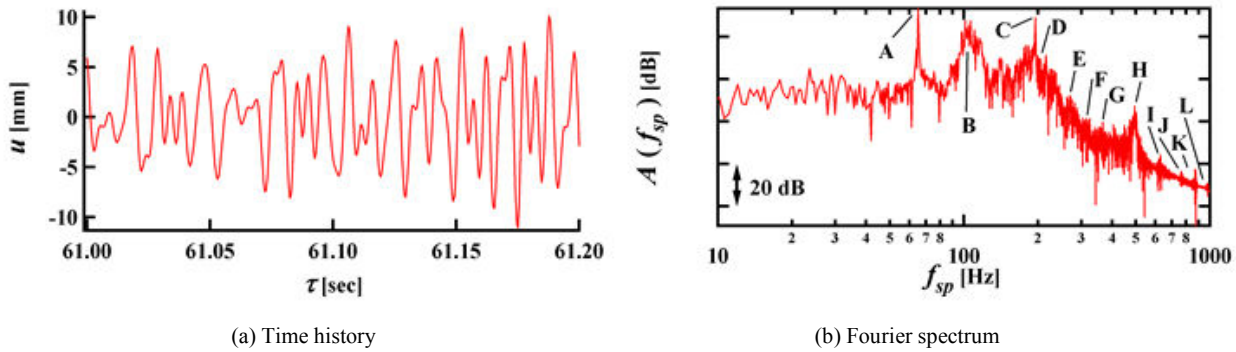


Fig. 8 Chaotic response of shock absorbing structure under large force amplitude ($f_{ex}=64.95\text{Hz}$, $|F_{max}|=4900\text{N}$)

Fig. 7 (a) shows the time history of the Fourier spectrum in Fig. 7 (b) under large force amplitude $|F_{max}|=4899\text{N}$. Under the large input, the time history is distorted complicatedly. Thus, many super harmonic, sub-harmonic and ultra-sub-harmonic components of the excitation frequency appear in the Fourier spectrums. The components of the typical peaks from A to D in this spectrum are also listed Table I related with Fig. 7 (b). The peak A corresponds to the excitation frequency f_{ex} and the principal component of mode 6. The peak C is the 1:3 internal resonance between mode 6 and mode 10 as we found previously in Fig. 6 (b). The peaks B and D newly appear accompanying internal resonances as listed in the table in Fig. 7 (b). The peak B has the 3/2 ultra-sub-harmonic components of both the excitation frequency f_{ex} and the eigen frequency of mode 6. In the vicinity of this frequency, there are two eigen frequencies for modes 8 and 9. The modes 8 and 9 involve rigid rotating motions of the whole shock absorbing structure about z and x axes, respectively. Among these three eigenmodes, multiple internal resonances are generated around peak B. On the other hand, the frequency of the peak D corresponds to the eigen frequency of mode 18, which is the first bending mode of the steel panel (i.e. the lower skin). This frequency corresponds to the fifth super-harmonic components of the modes 8 and 9. Moreover, this frequency is also related to the 15/2 ultra-sub-harmonic component of excitation frequency f_{ex} . Therefore, among these three modes, the multiple internal resonances appear around peak D near 500Hz.

We can regard that there exist complicated nonlinear couplings including many internal resonances among multiple modes under large input.

Fig. 8 (a) shows a time history under slightly larger force amplitude $|F_{max}|=4900\text{N}$ than $|F_{max}|=4899\text{N}$ used in Fig. 7 (a). As can be seen in this figure, the time history loses periodicity and becomes a random-like and chaotic response. According to the related Fourier spectrum represented in Fig. 8 (b), the peaks as we focused on previously in Fig. 7 (b) change to be broader band. Further, number of the peaks in Fig. 8 (b) increase than those as we observed in Fig. 7 (b). For these peaks, we clarify the components as listed in the Table II related with Fig. 8

(b). As we can see in this table, many internal resonances are observed accompanying the couplings among multiple eigenmodes.

TABLE I
FREQUENCY COMPONENTS OF DYNAMIC RESPONSE OF SHOCK ABSORBING
STRUCTURE UNDER LARGE FORCE AMPLITUDE ($f_{ex}=64.95\text{Hz}$, $|F_{max}|$

=4899N)			
A	B	C	D
(6,1)	(6,3/2)	(6,3)	(8,5)
	(8,1)	(10,1)	(9,5)
	(9,1)		(18,1)

Next, we focus on the mode 10 (peak C in Fig. 8 (b)), which magnify the amplitudes of the double skins. In this mode, the internal air of the porous material plays a roll of a pneumatic spring. Under small input force, this mode cannot be found as shown in Fig. 5 (b). But, under large input force, there exist the complicated nonlinear and chaotic couplings between this mode and the super harmonic components of the mode from 6 having large deformation in the nonlinear concentrated springs. And then, coupled spectra between the multiple modes appear as peak C in Fig. 8 (b).

TABLE II
FREQUENCY COMPONENTS OF DYNAMIC RESPONSE OF SHOCK ABSORBING
STRUCTURE UNDER LARGE FORCE AMPLITUDE ($f_{ex}=64.95\text{Hz}$, $|F_{max}|$

=4900N)				
A	B	C	D	E
(6,1)	(6,3/2)	(6,3)	(11,1)	(13,1)
	(8,1)	(10,1)	(12,1)	
	(9,1)			
F	G	H	I	J
(14,1)	(15,1)	(8,5)	(19,1)	(22,1)
		(9,5)		
		(18,1)		
K	L			
(23,1)	(25,1)			

Next, by using the random-like time history as discussed previously in Fig. 8 (a), we calculate the largest Lyapunov exponent λ_{max} as shown in Fig. 9 by means of Wolf's algorithm [17], [18] to investigate the chaotic motions. In Fig. 9, the

vertical axis is the largest Lyapunov exponent λ_{\max} , while the horizontal axis is the embedded dimension e . The exponent almost converges to a constant positive value as the embedded dimension e increases. We can confirm the random-like motion in Fig. 8 (a) as chaos because the converged largest Lyapunov exponent λ_{\max} is positive. The embedded dimension e is about 10 when the largest Lyapunov exponent λ_{\max} converges. This implies that number of the dominant components of this chaotic motion is about 10. By considering number of the state variables about the dynamic motion, half of the embedded dimension e can be regarded as number of the dominant eigenmodes in the chaotic motion. Therefore, we can estimate number of the dominant modes is about 5.

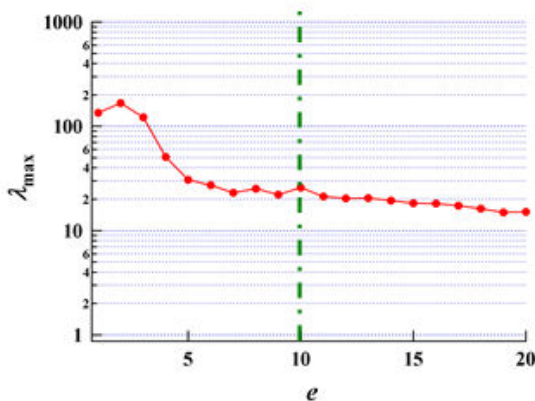


Fig. 9 Largest Lyapunov exponent of chaotic time history for shock absorbing structure

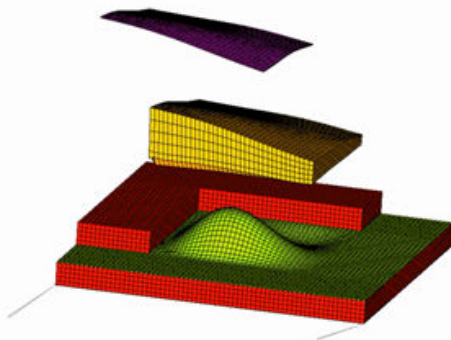


Fig. 10 A typical example of an instantaneous displacement distribution when chaotic motion appears

Fig. 10 shows a typical example of the instantaneous displacement distribution for the shock absorbing structure when the chaotic motion as shown in Fig. 8 (a) appears. When the response is the linear motion as shown in Fig. 5(a), the distribution can include only mode 6, which is the bouncing motion of the whole shock absorbing structure in y direction. As can be seen in Fig. 10 for the nonlinear and chaotic responses, there exist not only the motion of mode 6, but also

complicated coupled motions of modes 8 and 9 (i.e. the rotating motions of the whole shock absorbing structure with large deformation in the nonlinear concentrated springs), mode 10 (i.e. the bouncing motion of the cover plate in y direction), mode 18 (i.e. the first bending mode of the lower steel panel). These five modes correspond to the identified number of modes from Fig. 9. Moreover, according to Fig. 10, we can also find the other small motions, for example, modes 11 and 12 (i.e. rotating motions of the cover plate about x and z axes). This causes the incompleteness of the convergence for the largest exponent λ_{\max} against the embedded dimension e .

V. CONCLUSION

We investigated nonlinear dynamic characteristics of a shock absorbing structure including elastic panels, a porous material and nonlinear concentrated springs using our proposed fast computational method. As an example of the shock absorbing structure, we deal with a sponge sandwiched between double skins (i.e. a cover plate and a steel panel) supported by nonlinear concentrated springs. In this structure, the sponge plays a role of air cushion. The restoring force of the nonlinear springs has cubic nonlinearity and linear hysteresis damping. To compute the responses of the structure, we selected displacement vectors as common unknown variable to solve under coupled conditions in damping among the elastic materials, the porous material and the concentrated springs using finite element method. We computed approximate values of modal loss factors using Modal Strain and Kinetic Energy Method proposed previously by the authors. Further, to reduce degree-of-freedom, the discretized nonlinear equations in physical coordinate were transformed into the nonlinear ordinary coupled equations using normal coordinate corresponding to linear eigenmodes. We applied periodic forces on this structure to clarify qualitative basic dynamic behaviors by changing force amplitude.

We focused on investigations of the nonlinear motions under the 1:3 internal resonance condition between the bouncing mode having dominant deformation in the nonlinear concentrated spring and the mode with the rigid motion of the cover plate having large deformations of the pneumatic spring in the sponge. Under large input force, there exist the complicated nonlinear couplings among these modes and other eigenmodes in the shock absorbing structure. This leads to have the coupled spectra between multiple modes. Further, chaotic responses involving the multiple eigenmodes having multiple internal resonances were observed.

ACKNOWLEDGMENT

This work was supported by JSPS KAKENHI Grant Number 23560250.

REFERENCES

- [1] T. Yamaguchi, Y. Kurosawa and S. Matsumura, "FEA for damping of structures having elastic bodies, viscoelastic bodies, porous media and gas", *Mechanical Systems and Signal Processing*, Vol.21, pp.535-552, 2007.
- [2] T. Yamaguchi, Y. Kurosawa and H. Enomoto, "Damped vibration analysis

- using finite element method with approximated modal damping for automotive double walls with a porous material", *Journal of Sound and Vibration*, Vol.325, pp.436-450, 2009.
- [3] T. Yamaguchi, Y. Fujii, K. Nagai and S. Maruyama, "FEA for vibrated structures with non-linear concentrated spring having hysteresis," *Mechanical Systems and Signal Processing*, vol.20, pp.1905-1922, Nov. 2006.
- [4] T. Yamaguchi, Y. Fujii, T. Fukushima, T. Kanai, K. Nagai and S. Maruyama, "Dynamic responses for viscoelastic shock absorbers to protect a finger under impact force," *Applied Mechanics and Materials*, vol.36, pp.287-292, Oct. 2010.
- [5] T. Kondo, T. Sasaki and T. Ayabe, "Forced vibration analysis of a straight-line beam structure with nonlinear support elements," *Transactions of the Japan Society of Mechanical Engineers*, Vol.67, No.656C, pp.914-921, 2001.
- [6] E. Pesheck, N. Boivin, C. Pierre and S. W. Shaw, "Non-linear modal analysis of structural systems using multi-mode invariant manifolds", *Nonlinear Dynamics*, Vol.25, pp.183-205, 2001.
- [7] A. Craggs, "A finite element model for rigid porous absorbing materials", *Journal of Sound and Vibration*, Vol. 61-1, pp.101-111, 1978.
- [8] Y. Kagawa, T. Yamaguchi and A. Mori, "Finite element simulation of an axisymmetric acoustic transmission system with a sound absorbing wall", *Journal of Sound and Vibration*, Vol.53-3, pp.357-374, 1977.
- [9] H. Utsuno, T. W. Wu, A. F. Seybert and T. Tanaka, "Prediction of sound fields in cavities with sound absorbing materials", *AIAA Journal*, Vol.28-11, pp.1870-1875, 1990.
- [10] Y. J. Kang and S. Bolton, "Finite element modeling of isotropic elastic porous materials coupled with acoustical finite elements", *Journal of the Acoustical Society of America*, Vol.98-1, pp.635-643, 1995.
- [11] N. Attala, R. Panneton and P. A. Debergue, "A mixed pressure-displacement formulation for poroelastic materials", *Journal of the Acoustical Society of America*, Vol.104-3, pp.1444-1452, 1998.
- [12] M. A. Biot, "Theory of propagation of elastic waves in a fluid-saturated porous solid", *Journal of the Acoustical Society of America*, Vol.28-2, pp.168-178, 1955.
- [13] C. D. Johnson and D. A. Kienholz, "Finite element prediction of damping structures with constrained viscoelastic layers", *AIAA Journal*, Vol.20-9, pp.1284-1290, 1982.
- [14] B. A. Ma and J. F. He, "A finite element analysis of viscoelastically damped sandwich plates", *Journal of Sound and Vibration*, Vol.152-1, pp.107-123, 1992.
- [15] O. C. Zienkiewicz and Y. K. Cheung, *The finite element method in structural and continuum mechanics*, MacGraw-Hill, 1967.
- [16] E. L. Wilson, R. L. Taylor, W. P. Doherty and J. Ghaboussi, *Incompatible displacement methods, in numerical and computer methods in structural mechanics*, Academic Press, 1973.
- [17] T. Yamaguchi and K. Nagai, "Chaotic vibration of a cylindrical shell-panel with an in-plane elastic support at boundary", *Nonlinear Dynamics*, Vol.13, pp.259-277, 1997.
- [18] A. Wolf, J. B. Swift, H. L. Swinney and J. A. Vastano, "Determining Lyapunov exponents from a timeseries", *Physica* 16D, pp.285-317, 1985.